Rheology of dispersions containing non-spherical lipid particles

Zhulieta Valkova, Kristina Rusanova, Slavka Tcholakova ⬤, Diana Cholakova * ⬤, Nikolai Denkov ⬤

Department of Chemical and Pharmaceutical Engineering, Faculty of Chemistry and Pharmacy, Sofia University, 1 James Bourchier Avenue, Sofia 1164, Bulgaria

HIGHLIGHTS

- Novel procedure for modification of rheological properties of lipid dispersions is proposed.
- It involves formation of non-spherical lipid particles upon cooling of spherical droplets.
- Non-flowing, gel-like samples can be produced with ca. 11 vol% hexadecane drops.
- The optimal initial drop size for maximum viscosity increase is between ca. 4 and 13 μm.
- The process is applicable to a variety of lipids, incl. alkanes, alkenes and triglycerides.

GRAPHICAL ABSTRACT
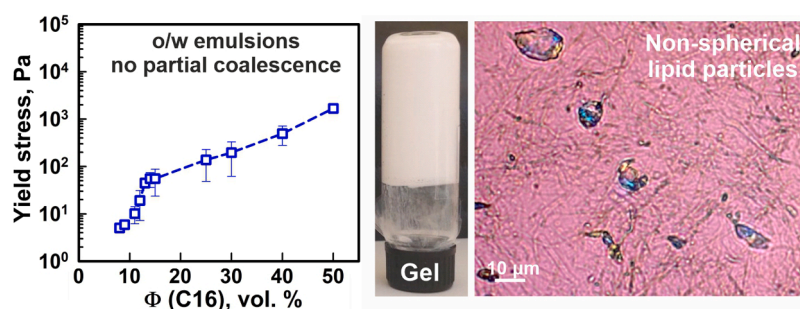
ARTICLE INFO

ABSTRACT

The rheological properties of disperse systems play a crucial role in the production of foods, cosmetics, and pharmaceuticals with desired characteristics. Emulsion viscosity can be increased through various methods, incl. increasing the oil volume fraction, incorporating rheological modifiers, or inducing partial coalescence between the droplets. It is well known that suspensions containing inorganic non-spherical particles often exhibit significantly higher viscosities when compared to those with spherical particles. The spontaneous drop self-shaping phenomenon in emulsions, first reported in detail by Denkov et al. (*Nature*, 2015, *528*, 392–395), enables the formation of fluid and frozen lipid particles with regular non-spherical shapes, including platelets, rods and fibers. In this study, we utilize this approach to prepare emulsions containing non-spherical frozen particles of various shapes and investigate their rheological properties. The effects of oil volume fraction, surfactant type, initial drop size and polydispersity are investigated. The results reveal that non-flowing, gel-like samples can be prepared at *ca.* 11 vol% oil fraction when the emulsion contains polydisperse droplets which acquire non-spherical shapes upon cooling. For comparison, more than *ca.* 65 vol% oil is needed to obtain similar rheological characteristics in samples containing spherical particles. Additionally, we demonstrate that the optimal drop size for gel preparation is $d_{32} \approx$ 4–13 μm. The obtained results are explained mechanistically, and guiding principles are provided for preparing emulsions with increased viscosities using this new approach.

1. Introduction

One of the key characteristics that must be carefully optimized in the production of foods, cosmetics, pharmaceuticals, liquid detergents, and other fluid products, used in our everyday life, is their rheological response. The flow behavior of all fluid products is essential not only for consumers perception but also for their manufacturing, visual appearance, stability, and overall performance [1–5]. Many of these products are essentially oil-in-water (o/w) emulsions, with typical examples being the mayonnaise, salad dressings, sauces, creams, moisturizers, lotions, paints, many pharmaceuticals, etc. [6–8].

Various approaches can be used to control the rheological properties of emulsions. For example, the increase of the oil fraction above the close packing fraction leads to the formation of deformed droplets and significant increase in the dispersion viscosity [9–11]. At low oil fractions, however, usually thickening agents are added into the aqueous phase to enhance its viscosity and provide the yield stress needed to suppress the gravitational separation (creaming) of the micrometer-sized oily droplets. Widely used thickeners include polysaccharides, such as xanthan gum, guar gum, agar and carrageenan; proteins, such as gelatin; or synthetic polymers [12–16]. Although generally considered as safe for consumers, the dietary intake of most of these substances should remain within a certain limit [17,18].

An alternative mechanism leading to significant increase in the viscosity of the emulsions is the appearance of partial coalescence upon drop crystallization [19–22]. Even though undesired for the long-term stability of emulsions, the partial coalescence instability, occurring in systems with semi-solid particles when a crystal from one particle protrudes and pierces another particle, can lead to the formation of a network of partially fused lipid particles. This process contributes significantly to the structure formation, sensory perception (fattiness, creaminess) and physicochemical properties (firmness, hardness, stability) of the final products. This approach is widely used in whipped toppings, ice cream and butter [20,23].

In the present study, we explore a different approach for preparing emulsions with non-Newtonian rheological properties. This approach relies on the preparation of emulsions containing non-spherical lipid frozen particles of various shapes, including hexagonal, triangular and tetragonal platelets, elongated rod-like particles (diameter ≈ 1–5 μm) and long thin fibers (diameter < 1 μm), see Fig. 1a. To produce these particles, we used the spontaneous drop self-shaping phenomenon which was studied in detail by our group in the last several years [24–27]. Briefly, the self-shaping process occurs upon cooling of oily drops composed of molecules capable of organizing into intermediate in stability phases. These phases should form between the completely disordered liquid phase and the fully ordered crystalline phase. Such phases are known to exist for most of the lipid molecules, for example – rotator phases in alkanes, Fig. 1c [28], and the α-polymorphic phase in triglycerides (TAGs) [29].

A second, equally important requirement for formation of non-spherical particles upon cooling, is that the surfactant adsorption layer should crystallize before the crystal nucleation inside the droplets'
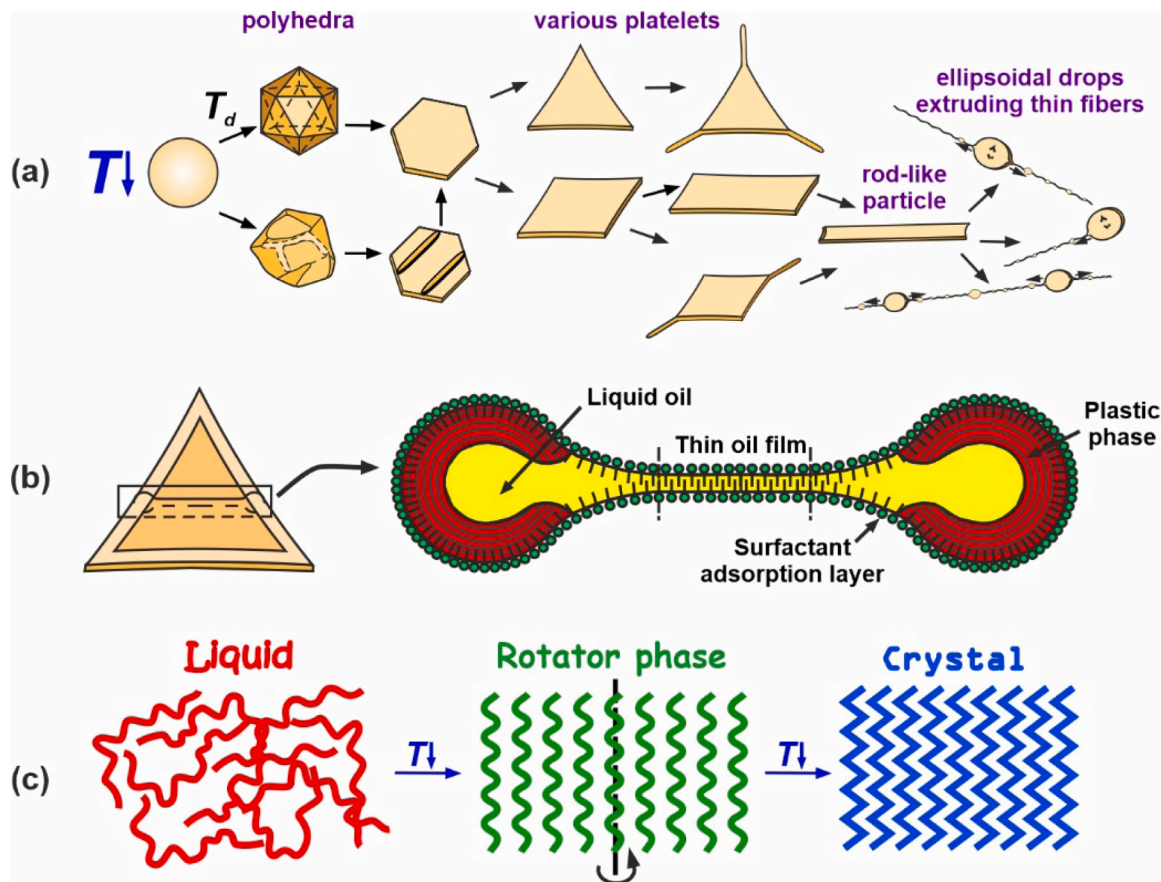

Fig. 1. (a) General drop shape evolutionary sequence followed by drops undergoing spontaneous shape changes upon cooling. (b) Schematics of the self-shaping mechanism showing deformed triangular platelet and its cross-section. The surface of the particle is covered by adsorbed surfactant molecules. To observe deformations upon cooling the surfactant molecules should be able to freeze before the bulk nucleation of the oil begins. Therefore, the frozen surfactant adsorption layer serves as a template for formation of ordered phase situated next to the drop surface (shown in red). This phase possesses the necessary mechanical strength to counteract the inner capillary pressure of the liquid oil (shown in yellow) remaining inside the deformed particle. (c) Schematic representation of the phase transitions exhibited by long-chain alkane molecules during cooling. Adapted from Refs [25,26,28].

interior begins [27]. Depending on the crystalline structure adopted by the lipid molecules, this requirement translates to different chain length differences (Δn) between the lipid molecule and the surfactant tail. For linear alkanes, drop shape deformations upon cooling are observed whenever $\Delta n \leq 3$ C-atoms and $\Delta n = z - x$, where z is the number of C-atoms in the alkane molecule and x is the number of C-atoms in the surfactant tail [27].

When both these requirements are fulfilled and the surfactant concentration is sufficiently high to allow the formation of a dense adsorption layer on the drop surfaces [30,31], the formation of numerous different drop shapes in fluid state is possible, despite the increased surface energy upon drop deformation. The self-shaping process has been demonstrated to be applicable for droplets containing various lipids, incl. alkanes, alkenes, long chain alcohols, triglycerides, mixtures thereof and other chemical substances [24,25,27,32,33]. Further details about the mechanism of the observed process can be found in the original papers, see also Fig. 1b [24–27,31]. We note that in a separate series of studies, Sloutskin et al. [34–36] proposed that similar deformations may occur also in systems having ultra-low interfacial tension which does not lead to energetic penalty once the surface area of the drops increases.

Although the self-shaping phenomenon has been widely studied with respect to its mechanism and application to numerous systems, a little is known about the bulk properties of the dispersions with non-spherical particles. In the pioneering work of Golemanov et al. [19] it was shown that the consistency of the dispersions containing 30 vol% hexadecane ($C_{16}H_{34}$), dispersed in aqueous solutions of different surfactants, depend significantly on the type of the surfactant included. For example, fluid samples were obtained with Brij 35 (polyoxyethylene lauryl ether), whereas gel-like samples were obtained with SDS (sodium dodecyl sulfate) and Brij 58 (polyoxyethylene hexadecyl ether). While the gelation in the sample stabilized by SDS was attributed to the presence of partial coalescence between the droplets, the significant increase in the viscosity of the Brij 58 containing sample was related to the appearance of non-spherical particles [19]. Note that the chain length differences for Brij 35 and Brij 58 are $\Delta n = 4$ and 0, respectively. Hence, drop deformations are not expected for Brij 35, whereas they appear for the emulsion containing Brij 58. No further studies were performed at that time to clarify the effects of the oil volume fraction, initial drop size and other relevant parameters on the rheological properties of the prepared emulsions.

In a more recent study by Reiner et al. [37], the authors used the self-shaping phenomenon to produce octadecane ($C_{18}H_{38}$) emulsions with non-spherical droplets stabilized by Brij S20 (polyoxyethylene octadecyl ether). The authors demonstrated that the viscosity of the 10 wt% octadecane emulsion decreased upon isothermal storage at temperatures below the bulk melting temperature of the octadecane. This result was related to the change in the shape of the frozen particles upon storage, namely – the initially long rod-like particles were argued to become shorter and more spherical over time. This result was interpreted as an appearance of drop recrystallization upon storage [37]. However, it was not explained why such recrystallization may appear in these systems and what is the mechanism behind it. Furthermore, the gravitational stability of the samples upon storage was not discussed.

These two previous studies, along with the numerous studies available in the literature about the role of the particle shape on the rheological properties of suspensions [38–46], demonstrate the significant role of the particle shape in the overall rheology response of the disperse systems. However, as seen from the short literature overview above, it remains unclear how the drop size distribution and the oil volume fraction in the initial emulsions, containing spherical non-interacting micrometer drops, would affect the rheological properties of the same emulsions after they are cooled to temperature, at which the drops acquire different non-spherical shapes. Note that the frozen lipid particles in our study are formed *in-situ* upon cooling of the emulsions. Therefore, the specific shape and aspect ratio of the frozen particles can change

significantly, depending on the initial drop size and polydispersity, surfactant used for emulsion stabilization, and oil volume fraction. The current study aims to answer the following related questions: (1) what is the minimal oil volume fraction required to obtain emulsions with non-zero yield stress after changing the drop shape upon cooling, (2) what is the effect of the initial drop size and polydispersity on the rheological properties of the dispersions containing non-spherical lipid particles, obtained *in-situ* upon emulsion cooling. Furthermore, this study aims to provide some guiding principles for utilization of this approach to modify the rheological properties of emulsions. With this aim in mind, we investigated the role of the oil fraction, surfactant type, initial drop size and polydispersity for the rheological properties of the cooled emulsions. Additionally, the long-term stability of the prepared gels was also monitored.

The obtained results are described in Section 3 below, after presenting the materials and methods in the following Section 2. The final Section 4 summarizes all main conclusions and proposes directions for future research.

2. Materials and methods

2.1. Materials

In the emulsions studied, we used hexadecane ($C_{16}H_{34}$, denoted as C_{16} throughout the text), a linear alkane with a purity of ≥ 99 %, purchased from Sigma-Aldrich, as the dispersed oily phase. The hexadecane, had a melting temperature $T_m = 18$ °C, and was used as received without further purification.

To stabilize the emulsions, we used nonionic surfactants from two main groups polyoxyethylene glycol alkyl ethers (trade name Brij, denoted as C_nEO_m) with $n = 12$ or 16 C-atoms and $m = 2, 4, 20$ or 23; and polyoxyethylene glycol (20) sorbitan monopalmitate (trade name Tween 40, denoted as $C_{16}SorbEO_{20}$). All surfactants were purchased from Sigma-Aldrich and used as received.

The concentration of the water-soluble surfactants in the aqueous phase was varied between 0.55 wt% and 2.2 wt% (with respect to the water), while the concentration of the oil-soluble surfactants in the oily phase ranged from 0.45 wt% to 1.8 wt% (with respect to the oil). These concentrations were selected to be sufficiently high, well above the critical micelle concentrations of the respective surfactants, to prevent drop-drop coalescence during the experiments and to ensure that sufficient amount of surfactant is available to cover the entire newly created surface area during the drop self-shaping upon cooling.

In some of the experiments we also added ethylene glycol (purchased from Valerus, Bulgaria). All aqueous solutions were prepared with deionized water purified by Elix 3 module (Millipore, USA).

2.2. Methods

2.2.1. Preparation of the studied emulsions

The hexadecane-in-water emulsions were prepared using three different emulsification procedures, depending on the desired drop size and polydispersity. In all cases, the water-soluble surfactants were dissolved into the aqueous phase, and the oil-soluble surfactants were dissolved into the oily phase prior to emulsification. Emulsification was performed at room temperature ($T \approx 25 \pm 2$°C), which is sufficiently high to ensure that the hexadecane will remain in a liquid state during the emulsification.

To obtain polydisperse emulsions with a mean Sauter droplet diameter $d_{32} \approx 4$ μm, we used a rotor-stator homogenizer (Ultra-Turrax T25, IKA, Germany). Note that $d_{32} = \sum_i d_i^3 / d_i^2$. The emulsions were prepared by first adding the required amount of the aqueous surfactant solution into a glass beaker. The oily phase was then gradually introduced in small portions while homogenizing with the rotor-stator device. Emulsification was carried out at 24,000 rpm for 5 minutes. Note

that we are working in the surfactant rich regime for emulsification, which ensures production of drops with similar sizes, irrespectively of the oil volume fraction [47]. The polydispersity of these samples, calculated as d_{V84}/d_{V50} [48], was approximately 1.46 ± 0.13, where d_{VX} represents the drop diameter at which X % of the oil volume is contained in drops smaller than d_{VX}. To check for possible influence of polydispersity on the results, we also studied samples with varying oil volume fractions prepared by diluting a more concentrated emulsion to the desired lower oil volume fraction. The results obtained from emulsions initially prepared at a specific oil volume fraction and those derived by dilution of a more concentrated sample were consistent within the frame of our experimental accuracy.

To prepare samples with smaller initial droplet sizes, d_{ini}, we used a high-pressure homogenizer (Panda Plus 2000, GEA Lab, Germany). First, the premix was homogenized using an Ultra-Turrax for 3 minutes at 13,500 rpm. The resulting emulsion was then passed once through the high-pressure homogenizer at a pressure of 200 bar. This method enabled us to prepare emulsions with a mean drop diameter below 1 µm [49].

The effect of drop size and polydispersity was also studied using monodisperse emulsion samples. These samples were prepared through membrane emulsification, using a laboratory microkit emulsification module from Shirasu Porous Glass Technology (SPG, Miyazaki, Japan). The emulsions were prepared by passing the oily phase through a porous glass membrane with a working area of approximately 3 cm^2 and a mean pore diameter of 2, 3 or 5 µm. Typically, this method produces droplets with diameters around three times larger than the pore diameter [50]. Further details about this emulsification technique can be found in Refs. [24–26]. The polydispersity for the monodisperse samples was $\approx 1.16 \pm 0.06$. The exact oil content of the emulsions prepared using this technique was determined through differential scanning calorimetry (DSC) analyses, see Section 2.2.4 below. If necessary, the emulsions were concentrated before the DSC measurements, by removing part of the aqueous phase after the drops creamed to the top of the container due to buoyancy. Samples with the desired oil content were then prepared by diluting the concentrated emulsions with the appropriate amount of aqueous phase, containing pre-dissolved surfactant, and used for further investigation.

2.2.2. Cooling of the bulk samples and long-term stability monitoring

After preparing the emulsion samples, approximately 10 g from each emulsion was transferred into glass bottles with a diameter of ca. 2 cm and a total volume of 20 ml. Typically, at least two bottles containing identical samples were prepared. To ensure reproducibility, two or three independent samples with the same compositions were prepared and studied separately. The results were with excellent agreement with one another.

The cooling of the bulk samples proceeded in the following way: the prepared samples with a temperature $\approx 25 \pm 2°C$ were placed in the refrigerator at $T \approx 5°C$. During the first hour of cooling, a gentle homogenization was applied by periodically shaking the bottles slightly (every 15–20 minutes) to prevent gravitational separation of the still-fluid droplets. The estimated average cooling rate of the emulsions was around 0.15 °C/min. The samples containing frozen hexadecane particles were then stored statically in the refrigerator until further inspection.

2.2.3. Rheological measurements

To characterize the rheological properties of the formed dispersions, we measured their yield stress, and their storage and loss moduli. These characteristics are determined in oscillatory experiments, in which the initial structure of the formed dispersions with non-spherical drops are weakly affected during the rheological test (in the linear regime and close to it). In addition, the apparent shear viscosities and the dynamic yield stress are determined in steady flow experiments.

The rheological tests were carried out using a Discovery Hybrid Rheometer HR-20 (TA Instruments, USA) with a parallel-plate geometry. The upper plate had a diameter of 40 mm, and the gap between the plates was set to 300 µm. Preliminary experiments were performed also with larger gaps and the obtained results were within the frame of our experimental accuracy, see Supplementary Figure S1. To prevent a possible wall slip between the sample and the plates during the experiments, ultra-fine sand paper of grade P1500 was glued to both the lower and upper plates (characteristic grain size ≈ 12 µm) [51]. All rheological measurements of the emulsions were conducted at 5°C after the samples had been stored for at least 24 hours at this temperature, unless otherwise noted explicitly. The samples were carefully transferred to the pre-cooled rheometer while maintaining the 5°C temperature. Additionally, before each rheology measurement, the samples were allowed to equilibrate for 3 minutes at 5°C. Note that the use of cone-plate geometry is not recommended for measuring the properties of such emulsions, because one cannot glue a sand paper on the cone surface to create appropriate roughness. Without surface roughness, the wall slip would affect strongly the results and it would be problematic to analyze them. In the current study we discuss mostly the yield stress and the rheological properties of the emulsions before they start flowing. Therefore, the non-homogeneous shear rate distribution, when parallel plate geometry is used, does not affect the final conclusions of the current study.

The storage and loss moduli, G′ and G″, of the emulsions were measured as a function of oscillation strain in amplitude sweep experiments. The applied strain was varied between 0.01 % and 1000 % at a fixed frequency of 1 Hz. From these measurements, we determined the viscoelastic properties of the samples, as well as its yield stress as the maximum point on the elastic stress vs oscillation strain curve [52]. The elastic stress was calculated as the product of the absolute oscillation strain (γ) and the storage modulus (G′).

The viscosities of the samples were measured as a function of the applied shear rate at 5°C in a flow ramp experiment. The shear rate was varied logarithmically in a stepwise manner from 0.1 to 100 s^{-1}, with a total of 31 data points recorded.

The error bars on the graphs throughout the text represent the standard deviation calculated from measurements performed on independently prepared samples, as well as from multiple measurements performed on a given sample.

2.2.4. Differential scanning calorimetry (DSC)

DSC experiments were conducted using a Discovery DSC 250 apparatus (TA Instruments, USA). A small amount of the sample (5–30 mg) was placed in an aluminum hermetic pan, carefully weighted, and hermetically sealed with an aluminum hermetic lid using a TZero sample press. The sealed sample was then placed in the DSC oven for the thermal measurements. Unless otherwise noted explicitly, the experimental protocol involved cooling the emulsion from 30°C to $-5°C$ at a constant rate of 5 °C/min. Note that only the dispersed hexadecane (C$_{16}$) undergo freezing transition, while the aqueous phase remains in a fluid state. After cooling, the samples were held isothermally for 5 minutes at $-5°C$, and then heated from $-5°C$ to 30°C at a rate of 2 °C/min. The obtained thermograms were analyzed using the build-in functions of the Trios data analysis software (TA instruments, USA) [53].

The DSC experiments were used to examine the crystallization profile of the studied samples and to determine the oil fraction in the emulsions prepared by the membrane emulsification technique, see Supplementary Figure S2. This was achieved by comparing the melting enthalpy of pure hexadecane ($\Delta H_m \approx 230$ J/g) with the melting enthalpy obtained from the emulsion samples. To validate this method, experiments were also performed on emulsion samples with known hexadecane volume fractions. The measured enthalpies showed excellent agreement with the expected values.

2.2.5. Optical microscopy observations and drop size measurements

Optical observations were performed with an AxioImager.M2m

microscope (Zeiss, Germany). Long-focus objectives with magnifications of $\times 20$, $\times 50$ and $\times 100$ were used in transmitted cross-polarized white light with an included compensator plate positioned after the sample and before the analyzer at a $45°$ angle relative to both the polarizer and analyzer. Under these conditions, isotropic fluid objects exhibit a characteristic magenta color, while birefringent objects display bright colors [24,25]. The samples were placed in glass capillaries with a rectangular cross-section, 100 μm in height and 2 mm in width (CM Scientific, Ireland) which were enclosed in a custom-made aluminum thermostatic chamber. The temperature of the chamber was controlled by a cryo-thermostat (Julabo CF-30). Further details can be found in Refs. [24–26]. Deformations of the drops in the bulk samples were inspected at $5°$C using a small amount of the already frozen concentrated sample. For better visualization, usually we pre-diluted the cooled bulk samples using a pre-cooled aqueous phase with identical composition as the one used for emulsion preparation.

The drop size distribution in the studied emulsions was determined from microscope images taken after emulsion preparation with $\times 50$ objective. For part of the samples, we also studied drop size distributions obtained after freezing and subsequent re-heating to temperature above the melting temperature of hexadecane. Microscopy images were taken at $T = 25°$C from the studied samples and analyzed using Image Analysis Module of Axio Vision software. The sizes of more than 10 000 individual droplets were measured and analyzed. For the samples with submicrometer droplets (prepared with the high-pressure homogenizer), we used laser diffraction equipment (Laser particle sizer Analysette 22 NanoTec, Fritsch, Germany) to determine the drop size distribution.

3. Experimental results and discussion

3.1. Effect of particle shape

To demonstrate the significant impact of the shape of frozen lipid particles on the viscosity of the prepared emulsions, we compared the viscosities of samples prepared with 40 vol% hexadecane, but stabilized by different emulsifiers, see Fig. 2a. The viscosities are measured at $5°$C, which is well below the bulk melting temperature of hexadecane, $T_m \approx 18°$C. Both samples contained polydisperse droplets with initial average sizes $d_{32} \equiv d_{ini} \approx 4 \pm 0.2$ μm, see Supplementary Figure S3. One of the samples was stabilized with C12-chain surfactants, $C_{12}EO_{23}$ and $C_{12}EO_4$, whereas the other sample was stabilized with longer-chain surfactants: the C16-chain water-soluble surfactant $C_{16}EO_{20}$ and oil-soluble surfactant $C_{16}EO_2$. The combination of a water-soluble surfactant added to the aqueous phase and an oil-soluble surfactant pre-dissolved in the oily phase was employed to ensure the formation of a dense adsorption layer that prevents partial coalescence during the freezing of droplets. As shown in the optical microscopy pictures and drop size distributions in Supplementary Figure S3, the droplets stabilized by the shorter-chain surfactants retained their sizes after one freeze-thaw cycle, while those stabilized by the C16-chain surfactants even decreased in size, $d_{32,1} \approx 1.9$ μm after one freeze-thaw cycle. This decrease is result from the action of different spontaneous self-emulsification mechanisms studied before [48,54].

In the emulsion stabilized by C12-chain surfactants, the chain length difference between the surfactant and the oily molecules is $\Delta n = 4$. Therefore, no drop shape deformations upon cooling are expected, see Introduction section above [25,27]. Indeed, no shape transformations were observed, and all droplets preserved their spherical shape after
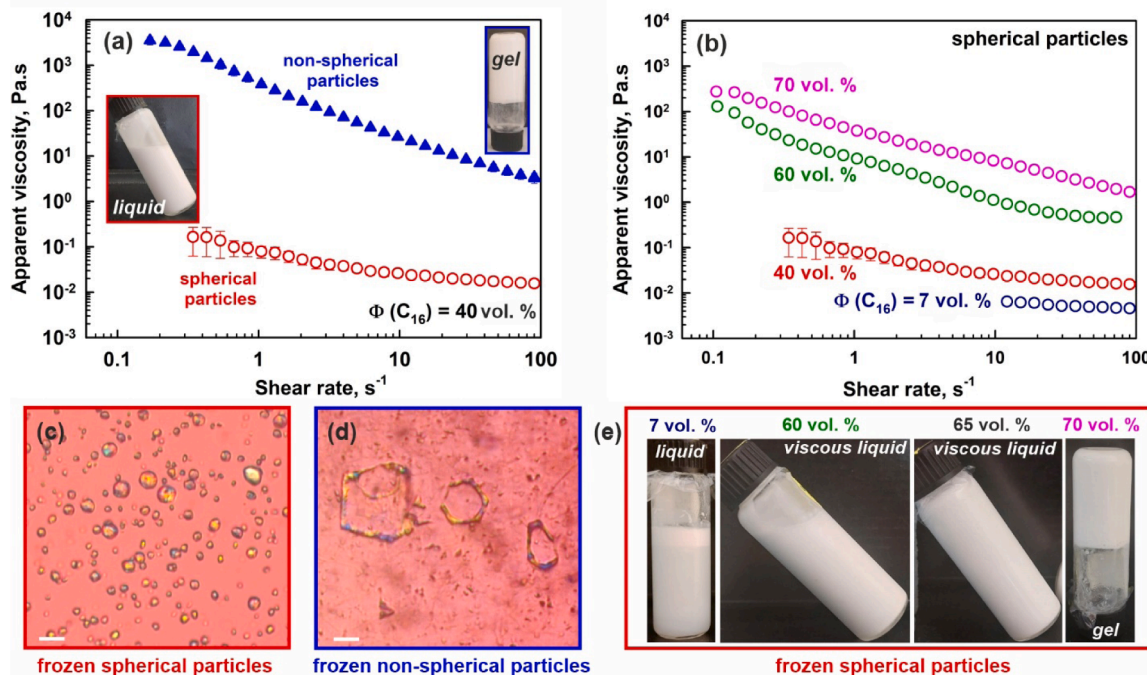

Fig. 2. (a) Apparent viscosity as a function of shear rate for 40 vol% C_{16} emulsions stabilized with different nonionic surfactants. Red empty circles: samples where drops freeze into spherical shapes, stabilized by 1.8 wt% $C_{12}EO_4$ and 2.2 wt% $C_{12}EO_{23}$. Blue filled triangles: samples where drops acquire non-spherical shapes upon cooling, stabilized by 1.8 wt% $C_{16}EO_2$ and 2.2 wt% $C_{16}EO_{20}$. Inset: images of the bulk emulsions taken after 24 h storage at $5°$C. (c,d) Optical microscopy images of solid particles observed in the two different emulsions with Φ (C_{16}) = 40 vol%. Spherical particles are seen in C12-chain stabilized C_{16} drops (c), whereas non-spherical particles are resent in C16-chain stabilized drops (d). Scale bars = 10 μm. (b) Viscosity of emulsions with spherical particles prepared with varying hexadecane volume fractions as denoted on the figure. The samples are stabilized by 1.8 wt% $C_{12}EO_4$ and 2.2 wt% $C_{12}EO_{23}$ surfactants. Viscosity increases with the oil content, but even at 70 vol% C_{16} it remains lower compared to the viscosity of the 40 vol% sample with non-spherical particle. (e) Macroscopic images of the samples shown in (b), $T = 5°$C. Gravitational instability (creaming) is observed in the 7 vol% sample. The studied samples are prepared by Ultra-Turrax homogenization and contain polydisperse droplets with an average drop diameter $d_{ini} \approx 4 \pm 0.2$ μm (measured at $25°$C, before freezing), see also Supplementary Fig. S3.

freezing, see Fig. 2c. In contrast, the emulsion stabilized by $C_{16}EO_2$ and $C_{16}EO_{20}$ (where $\Delta n = 0$) contained non-spherical frozen particles with various shapes, including rods and fibers, triangular and hexagonal platelets, and other non-spherical forms, Fig. 2d. This variety in shapes is due to the polydispersity in droplet sizes within these emulsions (polydispersity $= d_{V84}/d_{V50} \approx 1.46 \pm 0.13$). Depending on the initial droplet diameter, the transformations progressed through different stages of the general drop shape evolutionary sequence before freezing [24,25].

The significant difference in the shape of the frozen lipid droplets has a profound impact on the viscosities of the two samples, as illustrated in Fig. 2a. The emulsion stabilized by surfactants that do not induce shape transformations of the droplets upon cooling remains completely liquid after 24 hours of storage at 5°C with a viscosity remaining practically the same as the one measured when the drops are in a liquid state, see Supplementary Figure S4a. In contrast, the sample with non-spherical particles transforms into a non-flowing gel. The viscosities measured at a shear rate of $0.03 \ s^{-1}$ reveal a difference of over four orders of magnitude between the two samples, $\eta \approx 2000 \ Pa.s$ for the sample with non-spherical particles, whereas $\eta \approx 0.16 \ Pa.s$ for the sample with spherical particles. Both samples exhibit shear-thinning behavior.

To further demonstrate the effect of non-spherical drops on sample viscosity, we prepared emulsions using C12-chain surfactants at varying oil volume fractions. Samples containing spherical frozen particles with 60–65 vol% hexadecane appeared as viscous liquids after storage at low temperature, whereas 70 vol% oil concentration was required to produce a non-flowing gel-like sample, see Fig. 2b,e. Note that 70 vol% C_{16} is very close to the close packing volume fraction of polydisperse spheres

[8]. However, even in this case, the measured viscosity was still over 10 times lower compared to the viscosity of the 40 vol% sample stabilized by $C_{16}EO_{20}$ and $C_{16}EO_2$, which exhibited non-spherical particles upon cooling. The yield stress τ_y, calculated as the maximum in the elastics stress ($G'\gamma$) *vs.* oscillation strain curve, for the 40 vol% sample with spherical particles was negligible, $\tau_y < 1 \ Pa$, whereas for the sample with non-spherical particles it was $\tau_y \approx 325 \ Pa$, see Supplementary Figure S4.

These results demonstrate clearly the primary role of the shape of frozen particles in viscosity buildup. Next, we investigated the effect of oil volume fraction on the viscosity of emulsions containing non-spherical frozen particles.

3.2. Role of hexadecane content

To study the effect of oil volume fraction on the rheological behavior of emulsions undergoing drop shape deformations upon cooling, we prepared a series of samples, stabilized by $C_{16}EO_{20}$ and $C_{16}EO_2$ surfactants with varying oil concentrations. The samples were prepared with rotor-stator homogenizer and contained polydisperse droplets with initial average diameter $d_{ini} \approx 4 \ \mu m$. The results of these experiments are presented in Fig. 3.

Relatively low viscous, freely flowing samples were obtained when the C_{16} volume fraction was $\Phi \leq 7 \ vol\%$. A significant increase in viscosity was observed for samples containing 8 vol% C_{16}. Increase in oil concentration 11 vol% resulted in the formation of highly viscous, non-flowing samples (note that 11 vol% corresponds to 8.7 wt%). The
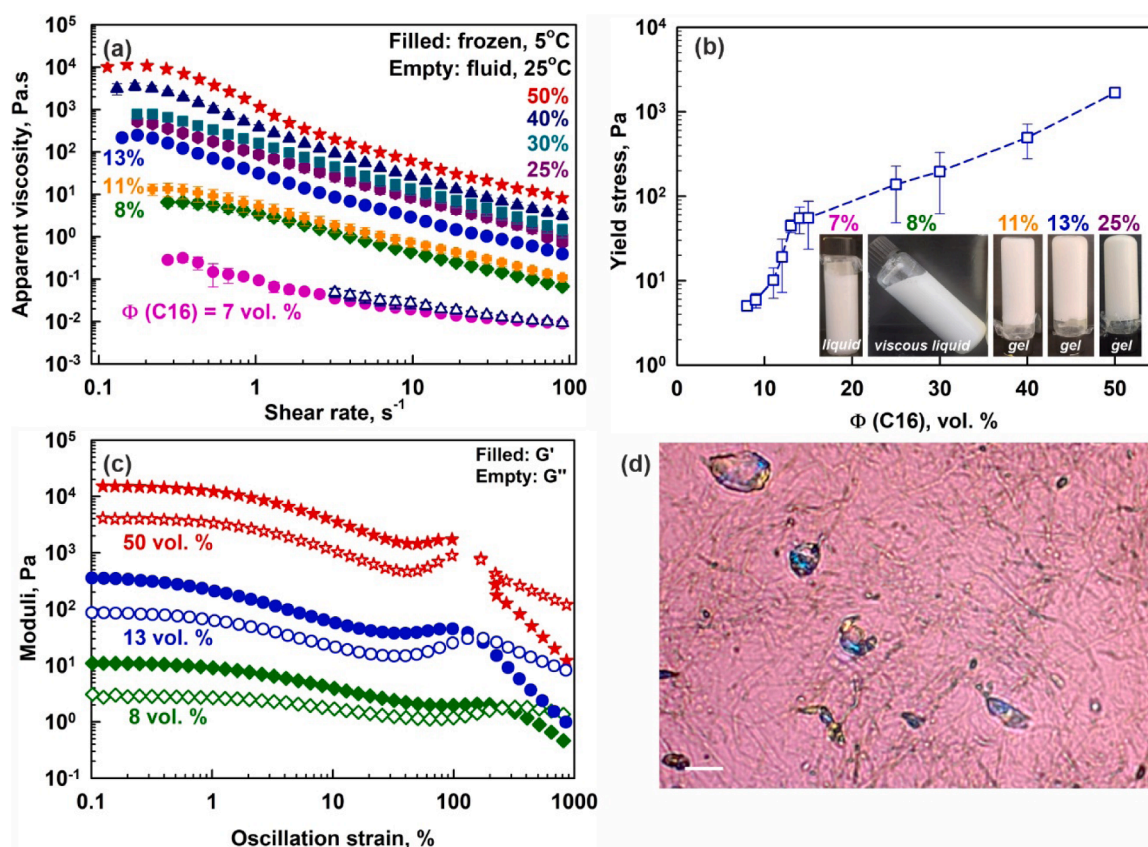

Fig. 3. Rheological properties of hexadecane-in-water emulsions stabilized by 1.8 wt% $C_{16}EO_2$ and 2.2 wt% $C_{16}EO_{20}$. (a) Apparent viscosity as a function of shear rate for samples with different C_{16}contents as denoted on the graph. Empty blue triangles: measurement for 40 vol% sample, performed at 25°C. All other measurements (filled symbols) are performed at 5°C with samples stored for 24 h period at 5°C. (b) Yield stress as a function of the oil concentration. Inset – pictures of the bulk samples stored at 5°C. (c) Storage (filled symbols) and loss (empty symbols) moduli measured at 5°C in amplitude sweep experiments for 8 vol% (green diamonds), 13 vol% (blue circles) and 50 vol% (red stars) samples. (d) Microscopy image showing non-spherical frozen particles present in the sample with 11 vol% C_{16} at 5°C. The sample has been diluted in a cold $C_{16}EO_{20}$ solution before the imaging. The image is obtained at 5°C. Scale bar $= 10 \ \mu m$. The average initial drop size of the studied emulsions (measured at 25°C before the freezing) is $d_{ini} \approx 4 \ \mu m$.

viscosities of the samples increased further as the hexadecane volume fraction increased. A similar trend was observed for the yield stresses of these samples, see Fig. 3a,b.

The emulsions with $\Phi \geq 8$ vol% exhibited viscoelastic behavior, with the storage modulus G' exceeding the loss modulus G'' even at high strain values (up to ca. 100 %), see Fig. 3c. This rheological behavior is governed by the crowding effect of non-spherical particles capable of trapping the entire liquid phase, effectively transforming the sample into a non-flowing gel-like sample. Numerous threads, fibers and platelets were observed in the frozen samples, as shown in Fig. 3d.

The threshold concentration for the observed significant increase in sample viscosity is related to the number of structures with anisotropic shape formed within the sample. Once this threshold concentration is exceeded (≈ 11 vol%), the particles become jammed which results in the gelation of the dispersion. Note that this concentration is significantly lower than that required to form gel-like samples with spherical frozen particles, which occurs when the critical close packing fraction of polydisperse spheres is reached, i.e. at $\Phi \approx 70$ vol% as shown in Fig. 2e. Similar decrease in the maximal packing fraction has been previously shown in the literature for monodisperse suspensions of solid particles [55]. It is important to note that this threshold differs from the percolation threshold commonly used for colloidal gels, which denotes the point at which most particles interconnect to form a space-spanning, infinite-size cluster [56]. In the systems studied here, the particles retain their individuality, with no evidence of aggregation or partial coalescence.

Moreover, the presence of frozen non-spherical particles is critical for the increased viscosity of the emulsions. When samples are investigated at temperatures above the bulk melting temperature of the hexadecane, $T_m \approx 18°C$, they behave as freely flowing liquids, with viscosities several orders of magnitude lower than those measured at 5°C. As an illustration, the empty triangular symbols in Fig. 3a present the viscosity of the 40 vol% C_{16} emulsion measured at 25°C. All other measurements were performed at 5°C, where the oily droplets are frozen in non-spherical shapes. Note that the viscosity measured for the sample with fluid spherical drops is identical to the viscosity measured with the C12-chain stabilized samples containing either frozen spherical particles or fluid spherical droplets, see Supplementary Figure S4a. Furthermore, the coincidence of viscosities values obtained for the 7 vol% sample with frozen non-spherical particles and 40 vol% sample with fluid spherical droplets further show the excellent structuring ability of the deformed droplets.

The thixotropic behavior of the studied systems was also investigated, see Supplementary Figure S5. For the 30 vol% emulsion, a significant decrease in the apparent viscosity was observed after shear at high rates. Initially, the viscosity at a shear rate of 0.18 s^{-1} was 1330 Pa. s. Upon increasing the shear rate to 100 s^{-1} and subsequently reducing it back to 0.18 s^{-1}, the viscosity dropped to 120 Pa·s. A further 10-fold reduction occurred after a second up-and-down cycle, bringing the viscosity to ≈ 13 Pa.s, Supplementary Figure S5a. In contrast, the 40 vol% sample exhibited more robust viscoelastic properties. Its initial apparent viscosity measured at 0.18 s^{-1} was ≈ 6130 Pa.s, decreasing to ≈ 2500 Pa.s after one up-down ramp, with no significant changes after a second ramp, Supplementary Figure S5b. The oscillation experiments performed with consecutive up-and-down ramps revealed consistent elastic and viscous moduli, provided the strain remained within the linear viscoelastic region, i.e. up to approximately 1 %, Supplementary Figure S5c,d. However, when the applied strain was increased to 1000 %, a pronounced decrease in both G' and G'' values was observed, particularly in the 30 vol% sample, Supplementary Figure S5e. Notably, the trend of the storage modulus exceeding the loss modulus persisted under low oscillation strain conditions.

The experimental data obtained from the flow curves (stress vs shear rate) were used to determine the dynamic yield stress [57,58]. The obtained experimental results are shown in Supplementary Figure S6. As can be seen, the data for the yield stress, τ_y, determined from the flow curve followed the same trend as those determined in the oscillatory experiments. However, the absolute values of the yield stress from the flow curves are slightly lower than those determined in the oscillatory experiments. The latter comparison is in a good agreement with the results reported in Ref. [57] where it was shown that the value of the yield stress, determined from Herschel-Bulkley fit to a shear-rate sweep experiments, consistently gave the lowest yield stress among all methods compared. However, it is also shown in Ref. [57] that, independently of the used method for determination of the yield stress, its dependence on the oil volume fraction is very similar. Therefore, the absolute value of the yield stress can change depending on the method used for its measuring, but the specific experimental method would not affect the main conclusions in our study.

The critical oil volume fraction of 11 vol%, above which the emulsions have sufficiently high yield stress to prevent their flow under gravity, is caused by the drop elongation upon emulsion cooling. To estimate the aspect ratio of the frozen drops we can apply the equation given in Ref. [59] for the lower bound of the glass region of a homogeneous network of rods, which can be written as $r = 0.7/\Phi_{glass}$, where r is the aspect ratio of the rods and Φ_{glass} is the minimum percolation volume fraction. For our system, $\Phi_{glass} \approx 0.11$, which means that the aspect ratio of the non-spherical drops is ≈ 6.7 – a value which is in a good agreement with the image shown in Fig. 3d. Therefore, we can conclude that the observed gel formation in our systems is related to the formation of rod-like particles which are sufficiently crowded to provide a yield stress, due to the excluded volume interactions. There is no need to invoke attractive interactions between the frozen particles to explain the measured yield stress.

3.3. Effect of the initial drop size and polydispersity

The initial drop size determines the non-spherical shapes formed during the spontaneous deformations preceding drop freezing. Typically, smaller droplets evolve more easily, reaching the final stages of the evolutionary sequence and predominantly form elongated rod-like particles and thin fibers. In contrast, larger droplets tend to evolve into platelet shapes before reaching the freezing temperature [25]. This trend is illustrated in Fig. 4, which shows images of the fluid (top row) and frozen (middle row) non-spherical shapes obtained during the cooling of diluted samples in capillaries at 0.5 °C/min. The experiments were performed with diluted samples containing monodisperse droplets with initial diameters of ca. 9.5 μm and 18.5 μm (Fig. 4b,c), as well as with small droplets prepared with a high-pressure homogenizer, $d_{ini} \approx 0.35$ μm (Fig. 4a). As seen from the images, all the small droplets evolved into thin fibers upon cooling. The intermediate-sized drops also progressed through the final stages of the shape evolutionary sequence, while the larger 18.5 μm droplets primarily formed elongated tetragonal platelets under these conditions.

The shapes formed after freezing in bulk batches (approximately 10 ml per sample in a glass bottle, cooling rate ≈ 0.15 °C/min) with these samples were also investigated, see the third row of Fig. 4. The most significant difference between the shapes observed in the capillary experiments and those in the bulk samples were seen for the 18.5 μm drops. In the bulk samples, part of the drops acquired hexagonal non-spherical shapes, while others froze earlier in the drop shape evolution, forming bulkier polyhedral shapes. This variation is most probably related to the limited space available in the concentrated bulk samples, which restricts the development of regular non-spherical shapes. Nevertheless, the trend that smaller drops evolve more easily than larger ones was also observed in the bulk samples.

Next, we compared the rheological properties of the emulsion samples prepared with different initial droplet sizes, see Fig. 5 and Supplementary Figure S7. As expected, the yield stresses of all samples increased with the increase of the hexadecane content, see Fig. 5d. However, the absolute values of viscosity and yield stress for a given hexadecane content were strongly dependent on the initial drop size.
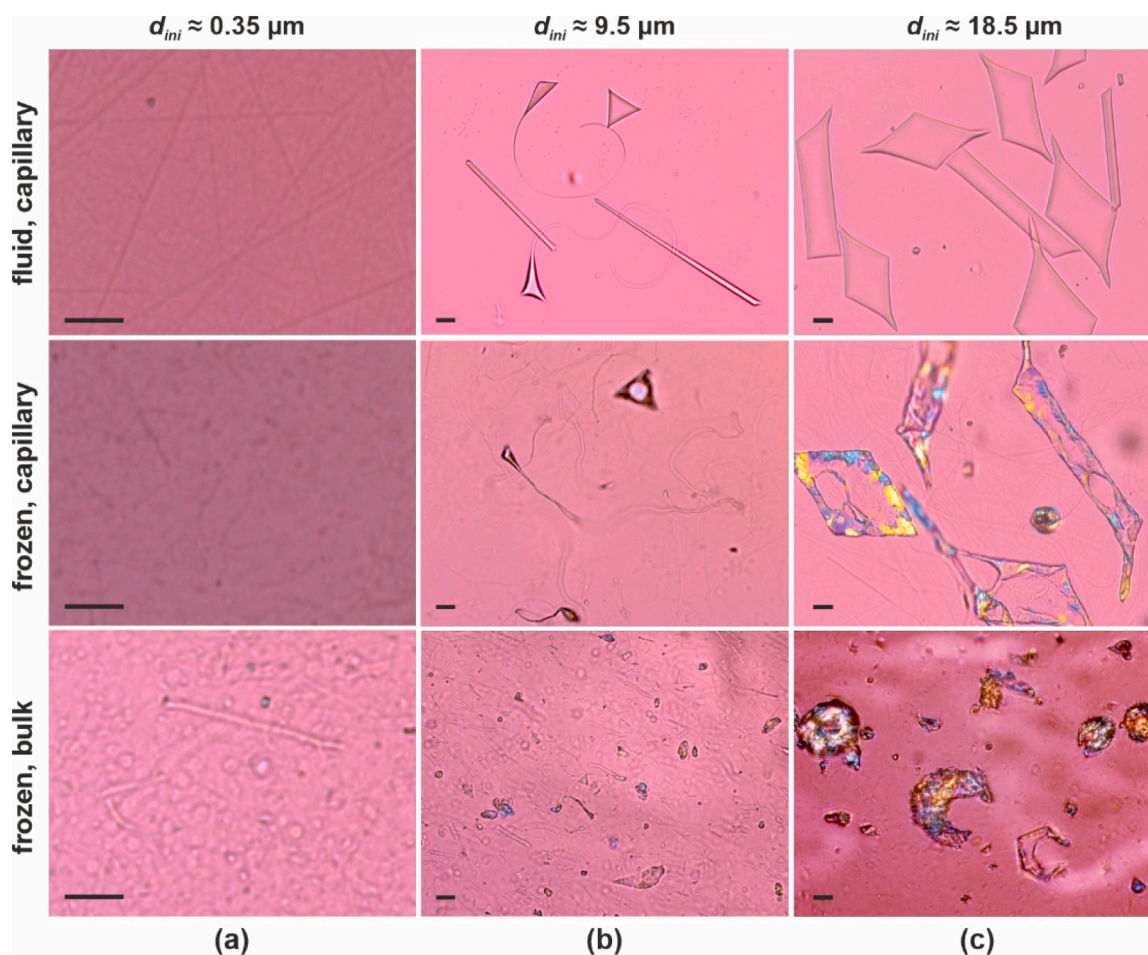
Fig. 4. Non-spherical fluid (top row) and frozen (middle row) particles obtained upon 0.5 °C/min cooling of hexadecane drops stabilized by $C_{16}EO_2$ and $C_{16}EO_{20}$ surfactants. The experiments were performed in glass capillaries with diluted samples, $\Phi \approx 0.1$ vol%. Drops evolve into different shapes depending on their initial drop size: (a) Thin fibers, $d_{ini} \approx 0.35$ μm. (b) Fibers, rods and triangular platelets, $d_{ini} \approx 9.5$ μm. (c) Tetragonal platelets with thick protrusions growing from their acute angles, $d_{ini} \approx 18.5$ μm. Bottom row: Images of samples with the same composition which have been frozen in bulk, $\Phi = 15$ vol%. The samples have been diluted in cold $C_{16}EO_{20}$ solution before imaging to $\Phi \approx 0.1$ vol%. Scale bars = 10 μm.

Samples containing the smallest droplets, $d_{ini} \approx 0.35$ μm, had the lowest viscosities. A sharp increase in their viscosity and yield stress was observed when the hexadecane content exceeded 25 vol%, Fig. 5a. However, even at 35 vol% C_{16}, the emulsion remained a highly viscous liquid, with its yield stress approaching the critical one for transitioning into a non-flowing, gel-like state. In contrast, the sample with monodisperse droplets of intermediate sizes, $d_{ini} \approx 9.5$ and 12.8 μm exhibited rheological properties identical to those of samples with 4 μm polydisperse droplets.

The increase of the drop size to $d_{ini} \approx 18.5$ μm leto somewhat unexpected result. The yield stress of the sample containing 15 vol% oil was comparable to that of samples with 4–13 μm droplets. Further increase of the hexadecane content, however, did not result in a corresponding rise in yield stress, instead it remained almost unchanged, and even slightly decreased, in the emulsions with Φ (C_{16}) between 15 and 35 vol%, Fig. 5d. This result was attributed to the limited space available in more concentrated samples, which prevented the droplets from adopting highly deformed, non-spherical shapes before their freezing. Note that the aspect ratio, defined as the ratio between the longest dimension of the non-spherical particle and the initial drop size can reach values between 10 and 100 when there is sufficient space available for drop deformations, see Fig. 4c and Figure 9 in Ref. [25]. In the bulk concentrated samples, the close proximity of individual droplets constrained these deformations, leading many droplets to freeze in near-spherical shapes with minimal deformations. The fraction of

minimally deformed frozen particles appeared to increase upon increase of the hexadecane content, see Supplementary Figure S8. As a result, these frozen near-spherical particles did not significantly contribute to the viscosity increase, which remained nearly constant, see Fig. 5c.

The conclusions about the 18.5 μm drops were in good agreement with the rheological properties of samples containing drops of identical size, but stabilized by $C_{16}SorbEO_{20}$ and $C_{16}EO_2$ surfactants instead of the $C_{16}EO_{20}$ and $C_{16}EO_2$ combination, see Fig. 6. Replacing the nonionic alcohol ethoxylated surfactant with linearly connected ethylene oxide units ($C_{16}EO_{20}$) with another nonionic surfactant, where the EO groups are attached at multiple positions to a sorbitane ring in the hydrophilic head ($C_{16}SorbEO_{20}$), has been shown to result in more constrained hexadecane drop deformations [25]. This is attributed to the formation of thicker plastic rotator phase layer in presence of $C_{16}SorbEO_{20}$ [53], which hinders the easy rearrangement of alkane molecules and drop deformations. Considering these trends, it was easy to explain why the yield stresses and viscosities of the samples with $d_{ini} \approx 18.5$ μm, stabilized by $C_{16}SorbEO_{20}$ and $C_{16}EO_2$, were even lower than those for samples stabilized by $C_{16}EO_{20}$ and $C_{16}EO_2$, see Fig. 6a. A higher number of nearly-spherical particles were observed in samples stabilized by $C_{16}SorbEO_{20}$ and $C_{16}EO_2$, which did not contribute for the viscosity increase, Fig. 6b. In contrast, when emulsions were prepared with smaller drop sizes, the drops were able to deform into rod-like particles and the bulk samples behaved similarly to those stabilized by $C_{16}EO_{20}$ and $C_{16}EO_2$ surfactants, see Fig. 6c,d.
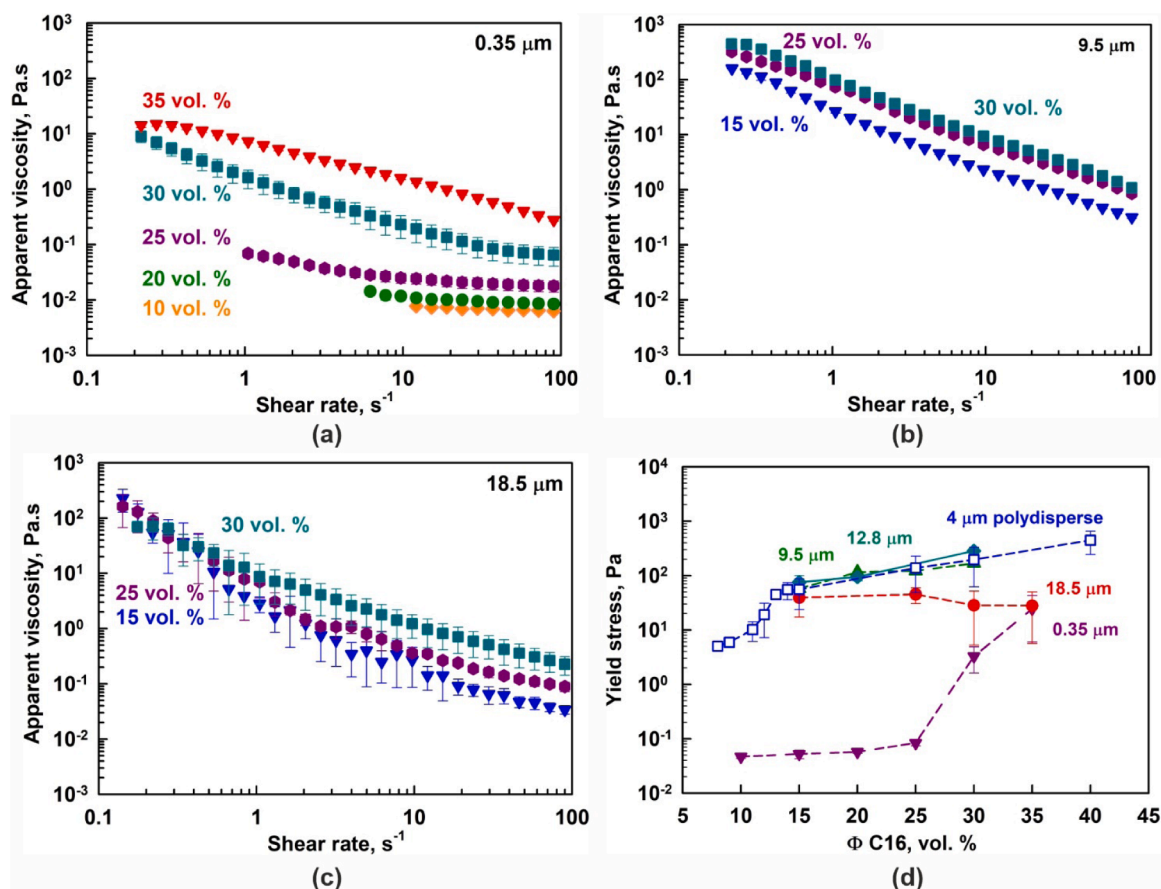
Fig. 5. Rheological properties of hexadecane-in-water emulsions with different initial drop sizes. All samples are stabilized by 1.8 wt% $C_{16}EO_2$ and 2.2 wt% $C_{16}EO_{20}$ surfactants. (a) Viscosities of samples prepared with high pressure homogenizer, $d_{ini} \approx 0.35$ µm. (b,c) Viscosities of samples prepared with the membrane emulsification technique: (b) $d_{ini} \approx 9.5$ µm, (c) $d_{ini} \approx 18.5$ µm. The hexadecane concentration in the studied emulsions is written on the graphs. (d) Yield stress as a function of the hexadecane fraction for the different samples studied: reversed dark blue triangles: 0.35 µm initial drop size, purple triangles: 9.5 µm drops, green diamonds: 12.8 µm drops, red circles: 18.5 µm drops. The empty blue squares show the data for polydisperse sample with $d_{ini} \approx 4$ µm.
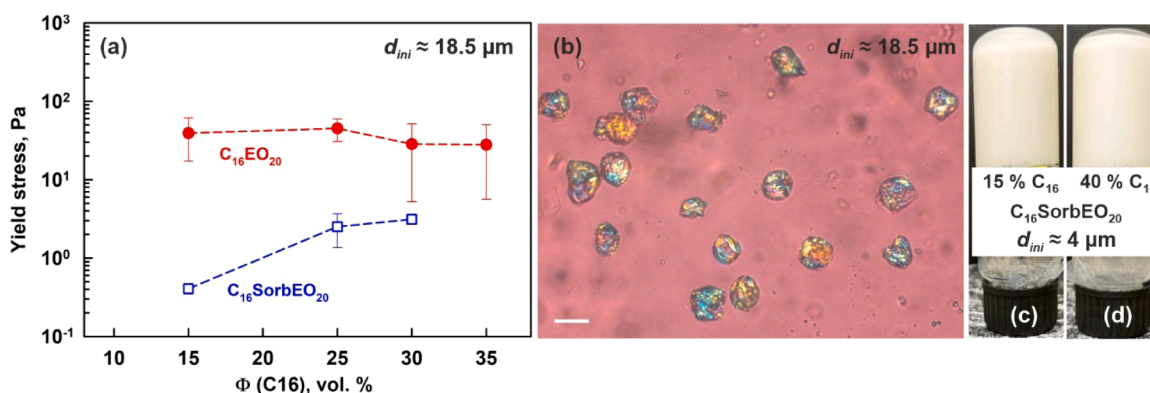

Fig. 6. Effect of surfactant type and initial drop size for the rheology of the frozen samples. (a) Comparison of the yield stresses measured at 5°C for bulk samples prepared with $C_{16}EO_{20}$ and $C_{16}EO_2$ surfactants, filled red circles and similar emulsions, but stabilized by $C_{16}SorbEO_{20}$ and $C_{16}EO_2$ surfactants, empty blue squares. The deformations with $C_{16}SorbEO_{20}$ are less pronounced compared to those with $C_{16}EO_{20}$, therefore the measured yield stresses are lower for samples stabilized by this surfactant. (b) Optical microscopy image of hexadecane frozen particles obtained after cooling of bulk emulsions with $\Phi = 25$ vol%. The initial drop size is $d_{ini} \approx 18.5$ µm and the sample is stabilized by $C_{16}SorbEO_{20}$ and $C_{16}EO_2$ surfactants. Scale bar = 20 µm. The sample has been diluted in cold $C_{16}SorbEO_{20}$ solution before imaging. (c,d) Images of the gel-like samples prepared with $C_{16}SorbEO_{20}$ and $C_{16}EO_2$ when the initial drop size is ≈ 4 µm. Polydisperse samples with: (c) $\Phi = 15$ vol% and (d) $\Phi = 40$ vol% are shown.

Interestingly, the viscosities of samples containing the smallest droplets, $d_{ini} \approx 0.35$ µm, stabilized by $C_{16}EO_{20}$ and $C_{16}EO_2$ surfactants, were significantly lower compared to those observed in samples with micrometer-sized droplets stabilized by the same surfactant combination. Even at a hexadecane content of 35 vol%, these samples did not form non-flowing gels. This result was unexpected, given that the droplets readily deformed into elongated, thin fibers, see Fig. 4a. Note that similar shapes were observed in polydisperse samples with an

average initial drop size of 4 µm, which exhibited significantly higher viscosities, Fig. 3d.

Two potential explanations could account for this significant difference. First, the thin fibers may lack the necessary mechanical strength to form a network with sufficient rigidity. Alternatively, as it is well known that the drop size decrease significantly increases the degree of undercooling required for crystallization [60,61], it is possible that not all small droplets crystallized under the studied experimental conditions, but part of them may remained in a fluid state. To clarify which explanation applies to our samples, we conducted additional experiments.

To exclude the possibility that the observed results were due to incomplete freezing of some droplets at 5°C, we prepared an emulsion sample following the same procedure but added 25 wt% ethylene glycol to the aqueous phase before emulsification. This modification allowed us to cool the sample to −18°C in a freezer without freezing the continuous aqueous phase, which could otherwise interfere with the small, deformed particles. The results from this experiment showed identical viscosities and yield stresses for samples prepared with and without ethylene glycol, indicating that prolonged storage at subzero temperatures did not increase the sample's viscosity. Furthermore, a DSC experiment confirmed that the melting enthalpy measured in an emulsion sample stored for 0.5 h at 5°C was the same as the enthalpy measured once the same sample was cooled to −10°C and stored at this temperature for 0.5 h before re-heating it. These results demonstrate that the lower viscosities observed in samples with smaller droplets are not related to incomplete drop freezing.

Therefore, the significant difference in properties between samples containing 0.35 µm droplets and those with 4 µm droplets is likely governed by the varying mechanical strength of the fibers and rod-like particles formed from droplets of different diameters. This difference is demonstrated in Supplementary Movies S1 and S2, which show how the two samples respond to mechanical agitation with a spatula. In the sample containing 40 vol% C_{16} and non-spherical particles derived from 4 µm drops, the gel structure remained intact after stirring, with no significant change in particle shape, see Supplementary Movie S1 and Supplementary Figure S9a,b. In contrast, when the same experiment was performed with smaller drops, a noticeable decrease in viscosity occurred after agitation although the initial sample contained 60 vol% C_{16}, and even after the sample was left undisturbed, the viscosity did not return to its original value. This reduction was caused by the partial breakage and shortening of the thin fibers, see Supplementary Figure S9c,d.

In conclusion, the experiments with droplets of different initial sizes showed that the most efficient viscosity buildup occurs when the drops have diameter between ca. 4 and 13 µm. These drops easily deform into long, rod-like particles which have the mechanical strength needed to form a non-flowing gel-like structure. Larger drops, however, form less deformed solid particles, which contribute to lower extent for the viscosity increase. In contrast, smaller drops do deform into fibers, but due to their small diameters, these fibers were fragile and prone to breaking into shorter pieces, which fail to entangle into a network, resulting in a lower viscosity of the bulk dispersion.

3.4. Stability of the gels upon storage

To evaluate the stability of the prepared viscous and gel-like dispersions containing non-spherical lipid particles, we monitored them during storage at 5°C. Illustrative images showing the appearance of the dispersions after several days or weeks storage are shown in Fig. 7. In all samples with $\Phi(C16) < 30$ vol%, syneresis was observed after a few days of storage. The amount of drained water increased over time and with decreasing hexadecane concentration. The viscous liquid sample with $\Phi(C16) \leq 10$ vol% remained in a liquid state and were easily re-homogenized by gentle shaking.

Samples with intermediate viscosities, $11 \leq \Phi(C16) \leq 25$ vol%, which initially appeared as non-flowing gels, transformed into highly
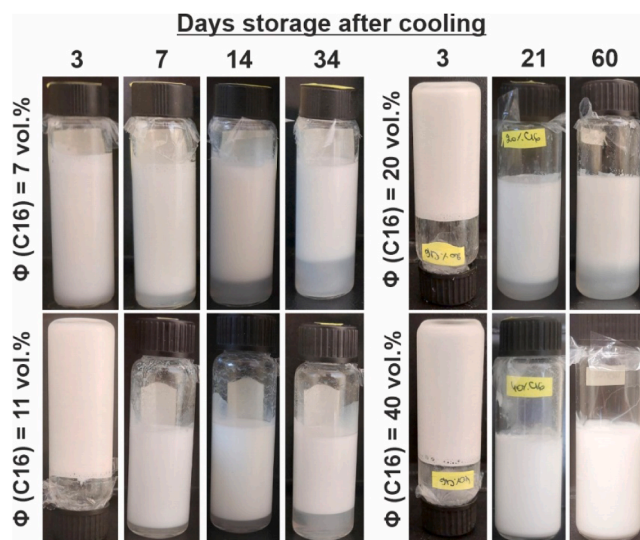

Fig. 7. Stability of bulk samples upon storage at 5°C. Macroscopic pictures of cooled emulsions prepared with polydisperse hexadecane drops ($d_{ini} \approx 4$ µm) stabilized by 1.8 wt% $C_{16}EO_2$ and 2.2 wt% $C_{16}EO_{20}$ upon storage are shown. The emulsions are prepared with different hexadecane volume fractions: 7, 11, 20 or 40 vol% as denoted on the figure. The numbers above the pictures show the number of days elapsed since the sample has been prepared and placed in the fridge.

viscous liquids after a few days of storage at low temperature. In contrast, the samples containing 30 vol% or more hexadecane retained their non-flowing gel consistency. Furthermore, little to no aqueous phase separation was observed in samples with 40 vol% or higher volume fraction of C_{16}, containing non-spherical alkane particles. Note that the water drainage is governed by the mechanical balance between the hydrostatic pressure, which is the driving force for the drainage, and the osmotic pressure of the dispersion with frozen particles, which causes the water suction from the surfactant solution into the dispersion [62]. Therefore, once a mechanical equilibrium is established between these two opposing forces, the rate of the water drainage slows down significantly [62]. This result is in agreement with the excellent thixotropic behavior exhibited by the 40 vol% sample, see Supplementary Figure S5b,d,f.

This result shows that while the small water molecules initially become entrapped between the deformed alkane particles as they freeze, they are not irreversibly trapped within the network and can escape from it over time due to gravity. No change in the non-spherical particles shapes was detected upon storage. The observed drainage can be prevented by adding a thickener to the aqueous phase [8,12–16].

4. Conclusions

The present study explores the impact of particle shape on the rheological properties of oil-in-water dispersions containing frozen hexadecane particles, formed in-situ upon cooling of spherical non-interacting liquid drops. Our findings demonstrate that dispersions, containing non-spherical frozen particles, exhibit significantly enhanced viscoelastic properties, when compared to emulsions with fluid spherical droplets or dispersions with frozen spherical particles. Note that the non-spherical particles preserve their individuality and the viscosity increase is not related to aggregation or partial coalescence between the droplets, while being created by the jamming of the particles with non-spherical shapes. Notably, a concentration of approximately 11 vol% C_{16} (≈ 8.7 wt%) was sufficient to produce a non-flowing, gel-like dispersion with a yield stress of about 10 Pa. The yield stress of the samples increased significantly with the hexadecane concentration, especially for samples prepared with ≥ 20 vol% C_{16}. In contrast, the

viscosity and the yield stress of dispersions containing fluid or frozen spherical particles remained significantly lower, until the 70 vol% C_{16} was reached.

Besides the oil concentration, the initial drop size has also a strong effect on the viscosity of the dispersions. The highest yield stresses were observed with samples containing non-spherical, highly deformed particles, prepared from initial spherical drops with diameter between ca. 4 and 13 μm. Larger initial drops limited the development of non-spherical shapes, causing many of the drops to freeze in nearly spherical forms, thereby not contributing significantly to the dispersion viscosity. On the other hand, submicrometer-sized droplets in emulsions exhibited significant drop deformations, forming a network of thin, entangled rod-like particles. However, these systems exhibited much lower viscosity, when compared to the dispersions prepared from 4 μm droplets. This behavior was attributed to the fragility of the thin rods, which were too weak to support the weight of the dispersion, breaking easily into smaller fragments and reducing the rheological properties of the systems.

The current study demonstrates how one could engineer dispersions with specific rheological profiles without using additional rheological modifiers. As the self-shaping process has already been shown to apply to a wide range of substances, incl. alkanes, alkenes, alcohols, tri-acylglycerols, and mixtures thereof [24–27,32,33], this novel method is highly versatile. Its potential applications span across various industries, including cosmetics and personal care products, food products, phase change materials, and many others.

CRediT authorship contribution statement

Valkova Zhulieta: Writing – original draft, Visualization, Validation, Investigation. **Rusanova Kristina:** Investigation. **Tcholakova Slavka:** Writing – review & editing, Supervision, Conceptualization. **Cholakova Diana:** Writing – review & editing, Writing – original draft, Visualization, Supervision, Investigation, Conceptualization. **Denkov Nikolai:** Writing – review & editing, Funding acquisition, Conceptualization.

Declaration of Competing Interest

The authors declare that they have no known competing financial interests or personal relationships that could have appeared to influence the work reported in this paper.

Acknowledgements

Appendix A. Supporting information

Supplementary data associated with this article can be found in the online version at doi:10.1016/j.colsurfa.2025.136284.

Data availability

Data will be made available on request.

References

[1] T. Tadros, Rheology of Dispersions: Principles and Applications, Wiley-VCH Verlag GmbH & Co. KGaA, 2010, https://doi.org/10.1002/9783527631568.
[2] M. Akhtar, B. Murray, E. Dickinson, Perception of creaminess of model oil-in-water dairy emulsions: influence of the shear-thinning nature of a viscosity-controlling hydrocolloid, Food Hydrocoll. 20 (2006) 839–847, https://doi.org/10.1016/j.foodhyd.2005.08.006.
[3] A. Tai, R. Bianchini, J. Jachowicz, Texture analysis of cosmetic/pharmaceutical raw materials and formulations, Int. J. Cosmet. Sci. 36 (2014) 291–304, https://doi.org/10.1111/ics.12125.
[4] M. Sikora, N. Badrie, A. Deisingh, S. Kowalski, Sauces and dressings: a review of properties and applications, Crit. Rev. Food Sci. Nutr. 48 (2008) 50–77, https://doi.org/10.1080/10408390601079934.
[5] V. Rai, N. Mishra, K. Yadav, N. Yadav, Nanoemulsion as pharmaceutical carrier for dermal and transdermal drug delivery: formulation development, stability issues, basic considerations and applications, J. Control. Release 270 (2018) 203–225, https://doi.org/10.1016/j.jconrel.2017.11.049.
[6] B. Khan, N. Akhtar, H. Khan, K. Waseem, T. Mahmood, A. Rasul, M. Iqbal, H. Khan, Basics of pharmaceutical emulsions: a review, Afr. J. Pharm. Pharmacol. 5 (2011) 2715–2725, https://doi.org/10.5897/AJPP11.698.
[7] E. Fredrick, P. Walstra, K. Dewettinck, Factors governing partial coalescence in oil-in-water emulsions, Adv. Colloid Interface Sci. 153 (2010) 1–2, https://doi.org/10.1016/j.cis.2009.10.003.
[8] D.J. McClements, Food Emulsions: Principles, Practices, and Techniques, second ed., CRC Press, Boca Raton, 2004, 10.1201/9781420039436.
[9] J. Giermanska, F. Thivilliers, R. Backov, V. Schmitt, N. Drelon, F. Leal-Calderon, Gelling of oil-in-water emulsions comprising crystallized droplets, Langmuir 23 (2007) 4792–4799, https://doi.org/10.1021/la070071c.
[10] R. Pal, Recent developments in the viscosity modeling of concentrated monodisperse emulsions, Foods 12 (2023) 3483, https://doi.org/10.3390/foods12183483.
[11] C. Liu, Z. Zheng, Y. Shi, Y. Zhang, Y. Liu, Development of low-oil emulsion gel by solidifying oil droplets: roles of internal beeswax concentration, Food Chem. 345 (2021) 128811, https://doi.org/10.1016/j.foodchem.2020.128811.
[12] D. Petri, Xanthan gum: a versatile biopolymer for biomedical and technological applications, Appl. Polym. 132 (2015) 42035, https://doi.org/10.1002/app.42035.
[13] P. Himashree, A. Sengar, C. Sunil, Food thickening agents: sources, chemistry, properties and applications - a review, Int. J. Gastron. Food Sci. 27 (2022) 100468, https://doi.org/10.1016/j.ijgfs.2022.100468.
[14] Y. Wei, Y. Guo, R. Li, A. Ma, H. Zhang, Rheological characterization of polysaccharide thickeners oriented for dysphagia management: carboxymethylated curdlan, konjac glucomannan and their mixtures compared to xanthan gum, Food Hydrocoll. 110 (2021) 106198, https://doi.org/10.1016/j.foodhyd.2020.106198.
[15] P. Shao, J. Feng, P. Sun, N. Xiang, B. Lu, D. Qiu, Recent advances in improving stability of food emulsion by plant polysaccharides, Food Res. Int. 137 (2020) 109376, https://doi.org/10.1016/j.foodres.2020.109376.
[16] E. Dickinson, Emulsion gels: the structuring of soft solids with protein-stabilized oil droplets, Food Hydrocoll. 28 (2012) 224–241, https://doi.org/10.1016/j.foodhyd.2011.12.017.
[17] L. Wu, C. Zhang, Y. Long, Q. Chen, W. Zhang, G. Liu, Food additives: from functions to analytical methods, Crit. Rev. Food Sci. Nutr. 62 (2022) 8497–8517, https://doi.org/10.1080/10408398.2021.1929823.
[18] E. Halmos, A. Mack, P. Gibson, Review article: emulsifiers in the food supply and implications for gastrointestinal disease, Aliment. Pharmacol. Ther. 49 (2019) 41–50, https://doi.org/10.1111/apt.15045.
[19] K. Golemanov, S. Tcholakova, N. Denkov, T. Gurkov, Selection of surfactants for stable paraffin-in-water dispersions, undergoing solid–liquid transition of the dispersed particles, Langmuir 22 (2006) 3560–3569, https://doi.org/10.1021/la053059y.
[20] E. Fredrick, P. Walstra, K. Dewettinck, Factors governing partial coalescence in oil-in-water emulsions, Adv. Colloid Interface Sci. 153 (2010) 30–42, https://doi.org/10.1016/j.cis.2009.10.003.
[21] L. Goibier, S. Lecomte, F. Leal-Calderon, C. Faure, , The effect of surfactant crystallization on partial coalescence in O/W emulsions, J. Colloid Interface Sci. 500 (2017) 304–314, https://doi.org/10.1016/j.jcis.2017.04.021.
[22] F. Thivilliers, E. Laurichesse, H. Saadaoui, F. Leal-Calderon, V. Schmitt, Thermally induced gelling of oil-in-water emulsions comprising partially crystallized droplets: the impact of interfacial crystals, Langmuir 24 (2008) 13364–13375, https://doi.org/10.1021/la802521f.
[23] H. Goff, Instability and partial coalescence in whippable dairy emulsions, J. Dairy Sci. 80 (1997) 2620–2630, https://doi.org/10.3168/jds.S0022-0302(97)76219-2.
[24] N. Denkov, S. Tcholakova, I. Lesov, D. Cholakova, S.K. Smoukov, Self-shaping of oil droplets via the formation of intermediate rotator phases upon cooling, Nature 528 (2015) 392–395, https://doi.org/10.1038/nature16189.
[25] D. Cholakova, N. Denkov, S. Tcholakova, I. Lesov, S.K. Smoukov, Control of drop shape transformations in cooled emulsions, Adv. Colloid Interface Sci. 235 (2016) 90–107, https://doi.org/10.1016/j.cis.2016.06.002.
[26] D. Cholakova, D. Glushkova, Z. Valkova, S. Tsibranska-Gyoreva, K. Tsvetkova, S. Tcholakova, N. Denkov, Rotator phases in hexadecane emulsion drops revealed by X-ray synchrotron techniques, J. Colloid Interface Sci. 604 (2021) 260–271, https://doi.org/10.1016/j.jcis.2021.06.122.
[27] D. Cholakova, A. Biserova, S. Tcholakova, N. Denkov, Self-shaping of triglyceride and alkane drops: similarities and differences, Colloids Surf. A 692 (2024) 134037, https://doi.org/10.1016/j.colsurfa.2024.134037.
[28] D. Cholakova, N. Denkov, Rotator phases in alkane systems: in bulk, surface layers and micro/nano-confinements, Adv. Colloid Interface Sci. 269 (2019) 7–42, https://doi.org/10.1016/j.cis.2019.04.001.
[29] D. Cholakova, N. Denkov, Polymorphic phase transitions in triglycerides and their mixtures studied by SAXS/WAXS techniques: in bulk and in emulsions, Adv.

Colloid Interface Sci. 323 (2024) 103071, https://doi.org/10.1016/j.cis.2023.103071.

[30] J. Feng, Z. Valkova, E.E. Lin, E. Nourafkan, T. Wang, S. Tcholakova, R. Slavchov, S. K. Smoukov, Minimum surfactant concentration required for inducing self-shaping of oil droplets and competitive adsorption effects, Soft Matter 18 (2022) 6729–6738, https://doi.org/10.1039.d1sm01326b.

[31] N. Denkov, D. Cholakova, S. Tcholakova, S.K. Smoukov, On the mechanism of drop self-shaping in cooled emulsions, Langmuir 32 (2016) 7985–7991, https://doi.org/10.1021/acs.langmuir.6b01626.

[32] D. Cholakova, Z. Valkova, S. Tcholakova, N. Denkov, S.K. Smoukov, Self-shaping" of multicomponent drops, Langmuir 33 (2017) 5696–5706, https://doi.org/10.1021/acs.langmuir.7b01153.

[33] D. Cholakova, D. Glushkova, S. Tcholakova, N. Denkov, Cold-burst method for nanoparticles formation with natural triglyceride oils, Langmuir 37 (2021) 7875–7889, https://doi.org/10.1021/acs.langmuir.0c02967.

[34] S. Guttman, Z. Sapir, M. Schultz, A. Butenko, B. Ocko, M. Deutsch, E. Sloutskin, How faceted liquid droplets grow tails, Proc. Natl. Acad. Sci. USA 113 (2016) 493–496, https://doi.org/10.1073/pnas.1515614113.

[35] S. Guttman, B. Ocko, M. Deutsch, E. Sloutskin, From faceted vesicles to liquid icosahedra: where topology and crystallography meet, Curr. Opin. Colloid Interface Sci. 22 (2016) 35–40, https://doi.org/10.1016/j.cocis.2016.02.002.

[36] O. Marin, M. Alesker, S. Guttman, G. Gershinsky, E. Edri, H. Shpaisman, R. E. Guerra, D. Zitoun, M. Deutsch, E. Sloutskin, Self-faceting of emulsion droplets as a route to solid icosahedra and other polyhedra, J. Colloid Interface Sci. 538 (2019) 541–545, https://doi.org/10.1016/j.jcis.2018.11.111.

[37] J. Reiner, T. Ly, L. Liu, H. Karbstein, Melt emulsions: influence of the cooling procedure on crystallization and recrystallization of emulsion droplets and their influence on dispersion viscosity upon storage, Chem. Ing. Tech. 94 (2022) 356–364, https://doi.org/10.1002/cite.202100143.

[38] I. Marti, O. Höfler, P. Fischer, E. Windhab, Rheology of concentrated suspensions containing mixtures of spheres and fibres, Original Contribution, Rhoel. Acta 44 (2005) 502–512, https://doi.org/10.1007/s00397-005-0432-9.

[39] F. van der Kooij, E. Boek, A. Philipse, Rheology of dilute suspensions of hard platelike colloids, J. Colloid Interface Sci. 235 (2001) 344–349, https://doi.org/10.1006/jcis.2000.7336.

[40] M. Solomon, D. Boger, The rheology of aqueous dispersions of spindle-type colloidal hematite rods, J. Rheol. 42 (1998) 929–949, https://doi.org/10.1122/1.550961.

[41] D. Heine, M. Petersen, G. Grest, Effect of particle shape and charge on bulk rheology of nanoparticle suspensions, J. Chem. Phys. 132 (2010) 184509, https://doi.org/10.1063/1.3419071.

[42] E. Boek, P. Coveney, H. Lekkerkerker, Computer simulation of rheological phenomena in dense colloidal suspensions with dissipative particle dynamics, J. Phys. Condens. Matter 8 (1996) 9509, https://doi.org/10.1088/0953-8984/8/47/053.

[43] F. Chinesta, G. Ausias, Rheology of Non-spherical Particle Suspensions, Elsevier Ltd, London, 2015, https://doi.org/10.1016/C2015-0-01208-4.

[44] J. Mewis, N.J. Wagner, Colloidal Suspension Rheology, Cambridge University Press, 2011, https://doi.org/10.1017/CBO9780511977978.

[45] N.J. Wagner, J. Mewis, Theory and Applications of Colloidal Suspension Rheology, Cambridge University Press, 2021, https://doi.org/10.1017/9781108394826.

[46] N.K. Reddy, Z. Zhang, M. Paul Lettinga, J.K.G. Dhont, J. Vermant, Probing structure in colloidal gels of thermoreversible rodlike virus particles: rheology and scattering, J. Rheol. 56 (2012) 1153–1174, https://doi.org/10.1122/1.4728335.

[47] S. Tcholakova, N.D. Denkov, D. Sidzhakova, I.B. Ivanov, B. Campbell, Interrelation between drop size and protein aggregation at various emulsification conditions, Langmuir 19 (2003) 5640–5649, https://doi.org/10.1021/la034411f.

[48] S. Tcholakova, Z. Valkova, D. Cholakova, Z. Vinarov, I. Lesov, N. Denkov, S. K. Smoukov, Efficient self-emulsification via cooling-heating cycles, Nat. Commun. 8 (2017) 15012, https://doi.org/10.1038/ncomms15012.

[49] S. Schultz, G. Wagner, K. Urban, J. Ulrich, High-pressure homogenization as a process for emulsion formation, Chem. Eng. Tech. 27 (2004) 361–368, https://doi.org/10.1002/ceat.200406111.

[50] N. Christov, D. Ganchev, N. Vassileva, N. Denkov, K. Danov, P. Kralchevsky, Capillary mechanisms in membrane emulsification: oil-in-water emulsions stabilized by Tween 20 and milk Proteins, Colloids Surf. A 209 (2002) 83–104, https://doi.org/10.1016/S0927-7757(02)00167-X.

[51] K. Golemanov, S. Tcholakova, N. Denkov, K. Ananthapadmanabhan, A. Lipids, Breakup of bubbles and drops in steadily sheared foams and concentrated emulsions, Phys. Rev. E 78 (2008) 051405, https://doi.org/10.1103/PhysRevE.78.051405.

[52] H.J. Walls, S.Brett Caines, A.M. Sanchez, S.A. Khan, Yield stress and wall slip phenomena in colloidal silica gels, J. Rheol. 47 (2003) 847–868, https://doi.org/10.1122/1.1574027.

[53] D. Cholakova, N. Denkov, S. Tcholakova, Z. Valkova, S.K. Smoukov, Multilayer formation in self-shaping emulsion droplets, Langmuir 35 (2019) 5484–5495, https://doi.org/10.1021/acs.langmuir.8b02771.

[54] Z. Valkova, D. Cholakova, S. Tcholakova, N. Denkov, S.K. Smoukov, Mechanisms and control of self-emulsification upon freezing and melting of dispersed alkane drops, Langmuir 33 (2017) 12155–12170, https://doi.org/10.1021/acs.langmuir.7b02048.

[55] S. Mueller, E.W. Llewellin, H.M. Mader, The effect of particle shape on suspension viscosity and implications for magmatic flows, Geophys. Res. Lett. 38 (2011) L13316, https://doi.org/10.1029/2011GL047167.

[56] M. Elbahri, M.K. Hedayati, S. Homaeigohar, M. Abdelaziz, 7 – Reawakening of plasmonic nanocomposites with the polarisonic reflective coloration: from metal to molecules, Front. Nanosci. 15 (2020) 185–214, https://doi.org/10.1016/B978-0-08-102515-4.00007-6.

[57] M. Dinkgreve, J. Paredes, M.M. Denn, D. Bonn, On different ways of measuring "the" yield stress, J. Non Newton. Fluid Mech. 238 (2016) 233–241, https://doi.org/10.1016/j.jnnfm.2016.11.001.

[58] P.C.F. Moller, J. Mewis, D. Bonn, Yield stress and thixotropy: on the difficulty of measuring yield stresses in practice, Soft Matter 2 (2006) 274–283, https://doi.org/10.1039/B517840A.

[59] M.J. Solomon, P.T. Spicer, Microstructural regimes of colloidal rod suspensions, gels, and glasses, Soft Matter 6 (2010) 1391–1400, https://doi.org/10.1039/B918281K.

[60] H. Nazir, M. Batool, F.J.B. Osorio, M. Isaza-Ruiz, X. Xu, K. Vignarooban, P. Phelan, Inamuddin, A.M. Kannan, Recent developments in phase change materials for energy storage applications: a review, Int. J. Heat. Mass Transf. 129 (2019) 491–523, https://doi.org/10.1016/j.ijheatmasstransfer.2018.09.126.

[61] L. Liu, J. Niu, J.-Y. Wu, Formulation of highly stable PCM nano-emulsions with reduced supercooling for thermal energy storage using surfactant mixtures, Sol. Energy Mater. Sol. Cells 223 (2021) 110983, https://doi.org/10.1016/j.solmat.2021.110983.

[62] N. Denkov, Mechanisms of foam destruction by oil-based antifoams, Langmuir 20 (2004) 9463–9505, https://doi.org/10.1021/la049676o.